

# TOWARDS SCALABLE NEWBORN SCREENING: AUTOMATED GENERAL MOVEMENT ASSESSMENT IN UNCONTROLLED SETTINGS

**Daphné Chopard\***

ETH Zurich

University Children’s Hospital Zurich

**Sonia Laguna \***

ETH Zurich

**Kieran Chin-Cheong \***

ETH Zurich

**Annika Dietz**

Children’s University Hospital Regensburg

**Anna Badura**

Children’s University Hospital Regensburg

**Sven Wellmann**

Children’s University Hospital Regensburg

**Julia E. Vogt**

ETH Zurich

## ABSTRACT

General movements (GMs) are spontaneous, coordinated body movements in infants that offer valuable insights into the developing nervous system. Assessed through the Prechtl GM Assessment (GMA), GMs are reliable predictors for neurodevelopmental disorders. However, GMA requires specifically trained clinicians, who are limited in number. To scale up newborn screening, there is a need for an algorithm that can automatically classify GMs from infant video recordings. This data poses challenges, including variability in recording length, device type, and setting, with each video coarsely annotated for overall movement quality. In this work, we introduce a tool for extracting features from these recordings and explore various machine learning techniques for automated GM classification.

## 1 INTRODUCTION

General movements (GMs) refer to spontaneous movements of the entire body observable in infants from early fetal life until approximately six months post-term (Einspieler & Prechtl, 2005). These movements include coordinated sequences of the arms, legs, neck, and trunk, with variations in intensity, force, and speed. GMs are inherently complex, variable, and fluid, and their quality can provide critical insights into the integrity of the developing nervous system. Assessing GM quality, known as the Prechtl General Movement Assessment (GMA), is a sensitive and reliable diagnostic tool for predicting the likelihood of cerebral palsy and other neurodevelopmental disorders (Einspieler & Prechtl, 2005). The types of movements predictive of later neurodevelopmental disorders vary significantly with age, and age-based distinctions are essential when studying newborns. From early fetal life until approximately two months post-term, GMs exhibit consistent writhing movements. Between 6 to 9 weeks post-term, these writhing patterns diminish, and fidgety movements emerge, persisting until around the middle of the first year of life, at which point intentional movements become predominant. Alterations in these movement patterns can indicate later disorders. While GMA is typically conducted in hospitals by specialized clinicians, there are too few trained experts to screen all newborns. This motivates the need to develop a tool for automatic and reliable classification of movements.

Initial attempts at addressing this challenge focused on computer-based approaches using feature extraction techniques (Baccinelli et al., 2020; Raghuram et al., 2022). However, recent advances in deep learning and computer vision have spurred the development of more sophisticated methods (Silva et al., 2021; Irshad et al., 2020). For instance, Reich et al. (2021) proposed to use a pose estimator, OpenPose, to extract skeletons and used these as input to a shallow multilayer neural network to discriminate between movements. Other deep learning solutions, e.g. by Schmidt et al.

\*Equal contribution. Correspondence to {dchopard, slaguna, kchincheong}@inf.ethz.ch.

(2019), work in controlled conditions. Despite their promise, these approaches often rely on controlled environments with fixed sensors and constant recording length, limiting their scalability and applicability in real-world clinical settings.

In this work, we present a preliminary study introducing a method to label key anatomical points, automatically process videos, and classify GMs based on the tracked anatomical points across videos, using a dataset from the Barmherzige Brüder Regensburg Hospital. The challenges posed by the variability in recording lengths and devices, the diversity of video scenarios (including both hospital and home environments), and the nature of the movement quality annotations—one per recording—are significant for reliable GM classification. Addressing these challenges is crucial to the generalization of an automatic GMA that can be effectively deployed in varied settings. The goal is to enable comprehensive newborn screening and follow-up studies by experts, ultimately improving the early detection and treatment of neurodevelopmental disorders.

## 2 DATASET AND METHODS

This work involves extracting features from specific anatomical landmarks of interest—so-called *keypoints (KP)*—in video frames (Section 2.4) to classify movement quality. We explore two means of acquiring the desired keypoints: 1) **Label & Track**, manually labelling specific KPs in a video frame (Section 2.2), and tracking their positions across the video (Section 2.2), as shown in the full pipeline illustrated in Figure 1, and 2) **Automatic Label**, automatically labeling the KPs in each frame, using the existing ML labeler AggPose Cao et al. (2022). The code<sup>1</sup> is publicly available.

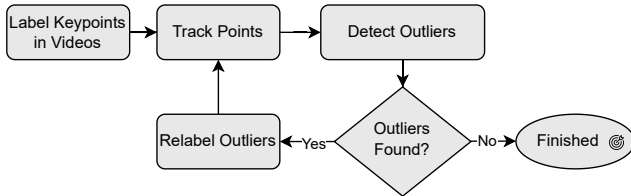


Figure 1: Flowchart of keypoint extraction pipeline after initial video resampling and cropping.

### 2.1 DATASET

This study includes 76 infant video recordings collected from the Barmherzige Brüder Regensburg Hospital. The dataset is highly heterogeneous, including videos recorded both at home and in hospital settings using various recording devices, resulting in differing resolutions and frame rates. There is also significant variability in camera angles and orientations, distance from subject to camera, infants’ clothing, and background types, among other factors.

The data is divided into two age-based groups according to the GM phase. The *early General Movement* group includes 39 infants with a postmenstrual age of 32 to 36 weeks (mean: 33 weeks), while the *late General Movement* group comprises of 37 infants with postmenstrual ages ranging from 49 to 59 weeks (mean: 53 weeks). Each sample is associated with a binary label reflecting the infant’s movement quality. Following Einspieler & Prechtl (2005), in the *early GM* group, which encompasses preterm and writhing GMs, labels distinguish between normal and poor movement repertoire. In contrast, the *late GM* group labels indicate the presence or absence of fidgety movements, with the presence of fidgety movements considered normal. To minimize bias and improve reliability, two trained physicians independently annotated the videos. In cases of disagreement, the recordings were reviewed jointly until a consensus label was reached. In the dataset, 24 infants in the early GM group exhibit poor repertoire, while 10 in the late GM group lack fidgety movements. Further details are included in Appendix A.

### 2.2 KEYPOINT RETRIEVAL TOOLS

#### 2.2.1 LABEL & TRACK

**Keypoint Labelling** We introduce a keypoint labelling tool based on the work from Doersch et al. (2022) to mark sets of key coordinates in the videos, which, along with point tracking, forms the

<sup>1</sup><https://github.com/chopardda/GMA>

backbone of the preprocessing pipeline. The tool allows labelling of extremities such as wrists and ankles—referred to as *extreme keypoints*, as well as additional joints such as elbows, hips, and knees—collectively referred to as *all keypoints*, totaling 17. In this study, three independent non-expert labellers manually labelled all keypoints for subsequent tracking. Full lists of relevant keypoints can be found in Figure 3, and Figure 2 a) provides an illustration of the tool.

**Point Tracking** For tracking labelled keypoints across video frames, we utilize the point tracking algorithm proposed by Doersch et al. (2022). This approach predicts the trajectory of each point by extracting dense feature representations for every frame, leveraging a cost-volume approach. Their model, TAP-Net, is designed to track arbitrary physical points on surfaces over video sequences. It is trained on a mix of synthetic and real-world datasets. The primary training datasets are synthetic, including TAP-Vid-Kubric, which contains simulated videos with physically realistic interactions between deformable and rigid objects, and TAP-Vid-RGB-Stacking, a robotic environment with teleoperated geometric shapes, focusing on challenges like tracking textureless and symmetric objects. These datasets provide perfect ground-truth point tracks, enabling TAP-Net to learn precise point tracking in complex, occlusion-prone scenarios. It uses a cost-volume-based architecture, inspired by optical flow methods, to track point motion across frames by comparing dense feature grids at query points. In particular, the cost volume measures the similarity between the feature of the tracked point in one frame and the features at all possible locations in subsequent frames, encoding the probability of the tracked point’s next position. A neural network then processes this cost volume to predict the tracked point’s location across frames. The network is trained with two objectives: (1) Point location regression, using Huber loss to estimate the query point’s position and ensure precise tracking, and (2) Occlusion classification, using cross-entropy loss to predict when the point is occluded, enabling the model to handle occlusion scenarios effectively. TAP-Net is validated and tested on real-world datasets like TAP-Vid-Kinetics, which includes diverse human actions and complex scenes, and TAP-Vid-DAVIS, which focuses on challenging segment and object tracking tasks.

### 2.2.2 AGGPOSE: AUTOMATIC LABEL

In addition to manually labelled keypoints, we evaluate as a benchmark an automatic labelling approach using AggPose (Cao et al., 2022), a deep aggregation vision transformer designed specifically for infant pose estimation and trained on a large-scale infant pose dataset. Unlike traditional convolutional models, AggPose discards convolutional layers in favour of a fully transformer-based architecture, leveraging multi-scale feature aggregation through a deep-layer fusion mechanism. This method enhances spatial information sharing across different resolution levels, improving the robustness of KP detection in challenging infant pose scenarios. In this study, we use AggPose to automatically label KPs in each frame of the video dataset, extracting the full set of coordinates across time. This method encompasses a total of 21 KPs, slightly larger than the prior approach. See Figure 2 c) for a visualization of the KPs.

## 2.3 DATA PREPROCESSING

Due to the heterogeneity of the data, a robust preprocessing and error correction pipeline is necessary to prepare the videos for machine learning model development. This subsection outlines the key steps in that process, with a graphical overview in Figure 1.

**Resampling and Extreme Keypoints Labelling** Preprocessing begins with homogenizing all the video data by resampling to 30 frames per second. Extreme keypoints are then labelled. If all required keypoints are not visible in the first frame, labelling occurs in subsequent frames where visibility is clearer.

**Video Cropping** Next, the extracted extreme keypoints are tracked and used to apply a rectangular crop per video. The crop is determined by the most extreme values of the tracked points in each video, with a 15% margin to ensure the infant consistently occupies a similar portion of the video frame. This normalization step is crucial for maintaining consistency in the input data for machine learning models.



Figure 2: **a)** The manual point labelling tool prompts the user to label either only *extreme keypoints* or *all keypoints*. **b)** The outlier detection tool displays potential unrealistic point movements and allows manual correction. **c)** Compared to manual labelling, some keypoints are missing (head top, ears, and nose), while others are added (eyes, hand and foot extremities, torso)—displayed in grey—when labelling automatically with AggPose.

**Outlier Detection** To address inaccuracies in the tracking algorithm in the *Label & Track* (See 2.2.1) approach, such as when points jump inappropriately due to occlusions or overlapping limbs, an outlier detection mechanism is applied.

The tool automatically flags any sudden and unrealistic movement of keypoints and prompts manual relabelling by the annotators, as shown in Figure 2 b). Specifically, we define such movements as coordinate changes that exceed 15 times the overall standard deviation for each keypoint. This threshold is set deliberately high to avoid flagging normal, natural movements, as well as fidgety movements that can inherently exhibit high magnitudes without indicating error. After relabelling, the affected keypoints are retracked. This process is iterated a fixed number of rounds, two in these results, as we observed only marginal improvements in performance after three rounds in the final detection task, or until no further outliers are detected, ensuring the accuracy of the tracked coordinates. In general, this outlier-detection process can be structured to run for a set number of iterations, until a defined performance tolerance is reached, or until no further outliers are identified, ensuring the accuracy of the tracked coordinates.

**Final Data Preparation** Prior to classification, the time series data must be homogenized. All video samples are split into fixed-length fragments corresponding to the shortest present recording, and zero-filling is applied to any occluded or missing coordinates. To prevent data leakage, we apply stratified sampling, ensuring that no single subject appears in both the training and testing datasets.

## 2.4 FEATURE EXTRACTION

We consider three feature sets from the tracked keypoints to perform the classification task:  $x$ - and  $y$ -coordinates of all keypoints and the angles between selected keypoints, based on Prakash et al. (2023).

Figure 3: List of *all* and *extreme* keypoints considered in this study for manual labelling, coloured by label on the right.

All Keypoints	Extreme
nose	
head bottom	
head top	x
left ear	
right ear	
left shoulder	
right shoulder	
left elbow	x
right elbow	x
left wrist	x
right wrist	x
left hip	
right hip	
left knee	x
right knee	x
left ankle	x
right ankle	x



Figure 4: Example of frame with labelled keypoints.

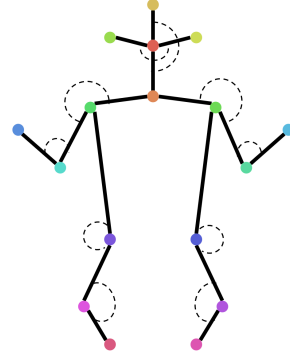


Figure 5: Illustration of the angle features. The dash lines show the angles that we compute in the set of angle features.

**Keypoint Coordinates** The  $x$ - and  $y$ -coordinates of all labelled keypoints are treated independently as separate input channels, and used as a simple representation of the keypoint positions across frames, as listed in Figure 3 and Figure 4.

**Keypoint Angles** The angles are calculated between pairs of keypoints to capture movement dynamics. We compute the dot product of vectors, normalizing by magnitudes, and applying a clipping function for valid angle calculations in radians, as illustrated in Figure 5. More precisely, given keypoints  $\mathbf{p}_1$ ,  $\mathbf{p}_2$ , and  $\mathbf{p}_3$  with coordinates  $(x_1, y_1)$ ,  $(x_2, y_2)$  and  $(x_3, y_3)$  respectively, we would like to compute the angle between  $\mathbf{p}_1$  and  $\mathbf{p}_3$  at middle point  $\mathbf{p}_2$ . Thus, we define

$$\mathbf{v}_1 = \begin{bmatrix} x_1 - x_2 \\ y_1 - y_2 \end{bmatrix}, \quad \mathbf{v}_2 = \begin{bmatrix} x_3 - x_2 \\ y_3 - y_2 \end{bmatrix}.$$

Then, the angle  $\theta$  between the two vectors can be computed as:

$$\theta = \arccos \left( \frac{\mathbf{v}_1 \cdot \mathbf{v}_2}{\|\mathbf{v}_1\| \|\mathbf{v}_2\|} \right),$$

where  $\mathbf{v}_1 \cdot \mathbf{v}_2$  is the dot product of the vectors and  $\|\mathbf{v}_1\|$  and  $\|\mathbf{v}_2\|$  are the magnitudes (or norms) of the vectors. Table 1 provides the list of the studied angle sets, which keypoints they are formed by, and a brief intuitive explanation. The angles are illustrated in 5. While there are more keypoints in the automatic labelling, the angle set is the same.

**Both** The combination of both coordinates and angles, shown as "both" in the results.

<b>p<sub>1</sub></b>	<b>p<sub>2</sub></b>	<b>p<sub>3</sub></b>	<b>Explanation</b>
head top	nose	head bottom	Head top to neck angle
right ear	nose	left ear	Right to left ear angle
left elbow	left shoulder	head bottom	Head to left shoulder angle
right elbow	right shoulder	head bottom	Head to right shoulder angle
left wrist	left elbow	left shoulder	Left elbow angle
right wrist	right elbow	right shoulder	Right elbow angle
left knee	left hip	left shoulder	Left hip angle
right knee	right hip	right shoulder	Right hip angle
left hip	left knee	left ankle	Left knee angle
right hip	right knee	right ankle	Right knee angle

Table 1: List of angle components used in the study with intuitive explanations.

## 2.5 CLASSIFICATION MODELS

This work explores three different classification models for GMA, using the extracted time series described in Section 2.4. 5-fold stratified cross-validation (CV) is performed across models to ensure robustness.

**1D Convolutional Neural Network (1D-CNN)** 1D-CNNs are a variant of the more common 2D convolutional neural network, which apply convolution operations to 1D signals, making them well-suited for processing time-series data. These networks have been shown to perform well when working with smaller labelled datasets and for specific applications (Kiranyaz et al., 2021).

**Long Short-Term Memory (LSTM)** LSTM networks (Hochreiter & Schmidhuber, 1997) are a type of recurrent neural network capable of exploiting the temporal aspect of our data by learning relevant context information from previously seen time points. LSTMs are ideal for handling time series and assessing whether longer temporal memory helps in recognizing and classifying infant’s general movements.

**Random Forest (RF)** RFs (Breiman, 2001) are powerful discriminative classifiers that perform well on a variety of datasets with minimal tuning (Biau & Scornet, 2016). It is an ensemble method that builds multiple decision trees trained on a random subset of data and combines their outputs to improve prediction accuracy and reduce overfitting. Although they do not explicitly account for the temporal structure of the data, their efficiency and accuracy make them a strong candidate for our classification tasks.

## 3 EXPERIMENTS AND RESULTS

### 3.1 IMPLEMENTATION DETAILS

We performed a grid search over the hyperparameter space for each of the three classifier types in Section 2.5, choosing the values that performed best in the evaluation. The final models were trained using these hyperparameters with 5-fold stratified CV, and the results from the held-out test set, with 20% of the data, were collected. On the *Label & Track* approach, the classification models used included a 1D-CNN with binary cross entropy (BCE) loss, learning rate of 0.00001, batch size 6, a fully-connected bottleneck with 150 features, and trained for 150 epochs. The LSTM used the BCE loss, learning rate 0.001, batch size 6, 3 layers, a hidden size of 64 and trained for 200 epochs. Finally, the random forest had 170 estimators. Moreover, using the *Aggpose* approach, the 1D-CNN had a learning rate of 0.0001, batch size of 4 and 150 features in the fully connected bottleneck trained for 50 epochs. The LSTM also used BCE loss learning rate 0.0001, batch size 4, 2 layers, a hidden size of 64 and trained for 50 epochs. Lastly, the random forest in this setup had 45 estimators. All experiments were run using 30 independent seeds on each individual set. Our models were implemented using pytorch v2.3.1 and scikit-learn v1.3.0. The final classification was

evaluated using accuracy, Area Under the Receiver Operating Characteristic Curve (AUROC), and Area Under the Precision–Recall curve (AUPRC).

### 3.2 RESULTS

Table 2: AUROC of various classifiers for GM classification across different keypoint labellers. The mean and standard deviation over 30 seeds is reported. Best result per model and labeller is bolded.

Keypoint Labeller	Input Features	Early GM Group AUROC			Late GM Group AUROC		
		RF	LSTM	CNN	RF	LSTM	CNN
#1	Coord.	0.6574 ± 0.19	0.6398 ± 0.16	0.7630 ± 0.19	0.3678 ± 0.25	0.4449 ± 0.23	<b>0.5804 ± 0.23</b>
	Angles	<b>0.8283 ± 0.13</b>	0.6617 ± 0.16	<b>0.8185 ± 0.14</b>	<b>0.5125 ± 0.25</b>	<b>0.6068 ± 0.21</b>	0.3770 ± 0.22
	Both	0.7878 ± 0.14	<b>0.6655 ± 0.16</b>	0.7876 ± 0.17	0.3763 ± 0.24	0.4007 ± 0.19	0.5371 ± 0.22
#2	Coord.	0.4907 ± 0.19	<b>0.6807 ± 0.17</b>	0.654 ± 0.19	0.4538 ± 0.24	0.4906 ± 0.24	0.5096 ± 0.20
	Angles	<b>0.6763 ± 0.15</b>	0.6324 ± 0.17	0.6050 ± 0.19	<b>0.6284 ± 0.20</b>	0.4902 ± 0.22	<b>0.6908 ± 0.22</b>
	Both	0.5737 ± 0.20	0.6088 ± 0.16	<b>0.6729 ± 0.20</b>	0.4899 ± 0.23	<b>0.5471 ± 0.18</b>	0.5888 ± 0.20
#3	Coord.	0.5874 ± 0.21	0.6176 ± 0.18	0.7493 ± 0.20	0.5179 ± 0.27	0.4286 ± 0.27	0.6196 ± 0.19
	Angles	<b>0.8105 ± 0.12</b>	0.5621 ± 0.16	<b>0.8138 ± 0.14</b>	<b>0.6267 ± 0.22</b>	<b>0.5351 ± 0.23</b>	<b>0.5915 ± 0.24</b>
	Both	0.7278 ± 0.18	<b>0.662 ± 0.21</b>	0.7846 ± 0.17	0.5651 ± 0.18	0.4762 ± 0.25	0.5392 ± 0.29
Mean	Coord.	0.5785	<b>0.6460</b>	0.7221	0.4465	0.4547	<b>0.5699</b>
	Angles	<b>0.7717</b>	0.6187	0.7458	<b>0.5892</b>	<b>0.5440</b>	0.5531
	Both	0.6964	0.6454	<b>0.7484</b>	0.4771	0.4747	0.5550
Automatic	Coord.	0.4780 ± 0.19	0.5721 ± 0.19	0.4643 ± 0.18	0.4001 ± 0.26	0.5436 ± 0.23	0.5628 ± 0.24
	Angles	<b>0.5076 ± 0.19</b>	<b>0.6112 ± 0.21</b>	0.4903 ± 0.15	<b>0.4381 ± 0.25</b>	<b>0.6586 ± 0.24</b>	<b>0.7156 ± 0.24</b>
	Both	0.4819 ± 0.17	0.5330 ± 0.21	<b>0.5101 ± 0.19</b>	0.4036 ± 0.24	0.6483 ± 0.26	0.5208 ± 0.29

Table 2 shows the results of the different classification models, for each labeller individually as well as averaged and labeled with AggPose, measured in AUROC. See Appendix B for a comprehensive overview of AUPRC and accuracy in each task. They demonstrate a variety of outcomes across age groups and feature sets, with no clear pattern indicating that one method is superior. However, the use of angle features, either isolated or combined, proves useful. Additionally, the early GM group shows significantly better overall results, showing a big difference in the difficulty of the task across age groups. Overall, the *Label & Track* approach performs comparably to the automatically labeled *AggPose* method. However, in a significant number of data groups, it demonstrates improved results, highlighting the positive impact of keypoint tracking. By incorporating temporal information from the time series, this approach enhances classification performance, whereas *AggPose* labels each keypoint in isolated frames, missing potential contextual cues. One of the key takeaways from this study is that despite the relatively small and heterogeneous dataset, our approach has shown success in automatically classifying GM in newborns, with average AUROCs of up to 0.8283 in certain scenarios, opening promising lines of research for GMA “in the wild”.

## 4 CONCLUSION AND FUTURE OUTLOOK

In conclusion, our study demonstrates that we can successfully predict GMA with a promising AUROC of up to 0.8283, with performance generally better for the early GM group. This highlights the potential of using automated methods to assess infant motor behaviour. Despite the challenges posed by diverse data sources and recording conditions in the data, our results show that automated GMA is feasible in real-world clinical settings. This is a significant step forward in the early detection of neurodevelopmental disorders. This study lays the groundwork for further advancements, emphasizing the need for larger datasets and more refined models and feature extraction approaches to capture the data complexities. Ultimately, the goal is to enhance early prediction of neurodevelopmental diseases, offering a valuable tool for clinicians, and ultimately improving patient care.

One of the key weaknesses of this study is the relatively small dataset, which limits the robustness and generalizability of our results, as indicated by relatively large standard deviations across folds. Moreover, the heterogeneity of the data makes the problem more challenging, while broadening its impact in the clinics. Expanding the dataset would allow us to explore more sophisticated methods,

such as Multiple Instance Learning (MIL), which could introduce interpretability by making predictions on a per-episode basis. Similarly, using Vision Transformers to directly process the videos could help better capture spatial and temporal patterns, further improving classification performance. Future work within the current dataset could focus on developing further features from the extracted keypoints and exploring other model classes to leverage the temporal structure in the task.

## ACKNOWLEDGMENTS

DC is funded from the Strategic Focal Area “Personalized Health and Related Technologies (PHRT)” grant #2021-911 of the ETH Domain (Swiss Federal Institutes of Technology), and SL and KC from the Swiss State Secretariat for Education, Research and Innovation (SERI), contract #MB22.00047. The authors would like to thank Ričards Marcinkevičs and Heike Leutheuser for their insights and discussions on the development of this manuscript.

## REFERENCES

- Walter Baccinelli, Maria Bulgheroni, Valentina Simonetti, Francesca Fulceri, Angela Caruso, Letizia Gila, and Maria Luisa Scattoni. Movidea: A software package for automatic video analysis of movements in infants at risk for neurodevelopmental disorders. *Brain sciences*, 10(4):203, 2020.
- Gérard Biau and Erwan Scornet. A random forest guided tour. *Test*, 25:197–227, 2016.
- L Breiman. Random forests. *Machine Learning*, 2001.
- Xu Cao, Xiaoye Li, Liya Ma, Yi Huang, Xuan Feng, Zening Chen, Hongwu Zeng, and Jianguo Cao. Aggpose: Deep aggregation vision transformer for infant pose estimation. *arXiv preprint arXiv:2205.05277*, 2022.
- Carl Doersch, Ankush Gupta, Larisa Markeeva, Adria Recasens, Lucas Smaira, Yusuf Aytar, Joao Carreira, Andrew Zisserman, and Yi Yang. Tap-vid: A benchmark for tracking any point in a video. *Advances in Neural Information Processing Systems*, 35:13610–13626, 2022.
- Christa Einspieler and Heinz FR Prechtl. Prechtl’s assessment of general movements: a diagnostic tool for the functional assessment of the young nervous system. *Mental retardation and developmental disabilities research reviews*, 11(1):61–67, 2005.
- Sepp Hochreiter and Jürgen Schmidhuber. Long short-term memory. *Neural computation*, 9(8):1735–1780, 1997.
- Muhammad Tausif Irshad, Muhammad Adeel Nisar, Philip Gouverneur, Marion Rapp, and Marcin Grzegorzec. Ai approaches towards prechtl’s assessment of general movements: A systematic literature review. *Sensors*, 20(18):5321, 2020.
- Serkan Kiranyaz, Onur Avci, Osama Abdeljaber, Turker Ince, Moncef Gabbouj, and Daniel J Inman. 1d convolutional neural networks and applications: A survey. *Mechanical systems and signal processing*, 151:107398, 2021.
- Varun Ganjigunte Prakash, Manu Kohli, Aragulla Prasad Prathosh, Monica Juneja, Manushree Gupta, Smitha Sairam, Sadasivan Sitaraman, Anjali Sanjeev Bangalore, John Vijay Sagar Kommu, Lokesh Saini, et al. Video-based real-time assessment and diagnosis of autism spectrum disorder using deep neural networks. *Expert Systems*, pp. e13253, 2023.
- Kamini Raghuram, Silvia Orlandi, Paige Church, Maureen Luther, Alex Kiss, and Vibhuti Shah. Automated movement analysis to predict cerebral palsy in very preterm infants: an ambispective cohort study. *Children*, 9(6):843, 2022.
- Simon Reich, Dajie Zhang, Tomas Kulvicius, Sven Bölte, Karin Nielsen-Saines, Florian B Pokorny, Robert Peharz, Luise Poustka, Florentin Wörgötter, Christa Einspieler, et al. Novel ai driven approach to classify infant motor functions. *Scientific Reports*, 11(1):9888, 2021.

William Thomas Schmidt, Matthew Regan, Michael C Fahey, and Andrew Paplinski. General movement assessment by machine learning: why is it so difficult? *Journal of Medical Artificial Intelligence*, 2(July):15, 2019.

Nelson Silva, Dajie Zhang, Tomas Kulvicius, Alexander Gail, Carla Barreiros, Stefanie Lindstaedt, Marc Kraft, Sven Bölte, Luise Poustka, Karin Nielsen-Saines, et al. The future of general movement assessment: The role of computer vision and machine learning—a scoping review. *Research in developmental disabilities*, 110:103854, 2021.

## A EXTENDED DATASET DESCRIPTION

In this section, we present additional details about our dataset to the best of our ability. Some details are not available to us, such as weight at video recording time for early GM group infants. Table 3 shows several demographic characteristics, as well as details about the videos themselves for both the early and late GM groups. Figure 6 provides histograms for the distributions of both video resolution and FPS for the early and late GM groups.

Table 3: Calculated demographic and video characteristics

Characteristic	Early GM Group	Late GM Group
Age at video recording (Days) (mean $\pm$ stddev)	30.9 $\pm$ 19.9	170.4 $\pm$ 24.8
Post-menstrual age at video recording (Days) (mean $\pm$ stddev)	231.5 $\pm$ 6.5	N/A
Corrected Age at video recording (Days) (mean $\pm$ stddev)	N/A	92.5 $\pm$ 17.4
Weight at video recording [g] (mean, stddev)	N/A	4148.2 $\pm$ 830.7
Video Length [s] (mean $\pm$ stddev)	409 $\pm$ 144	224 $\pm$ 93
FPS [min, max]	[30, 120]	[30, 120]
Extremely Preterm	16	15
Very Preterm	20	19
Moderate to Late Preterm	3	3
Not Preterm	0	0

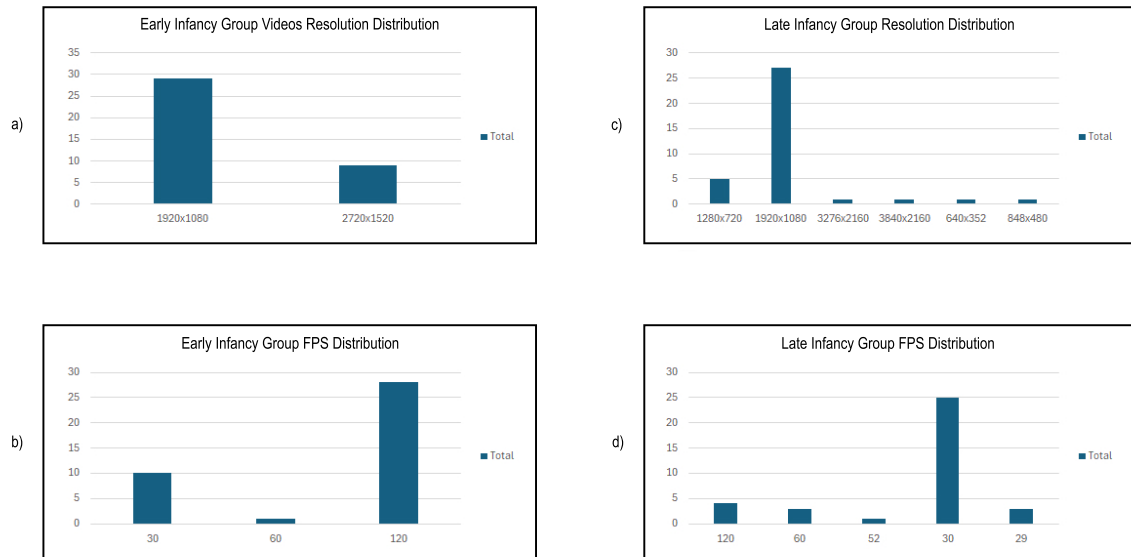


Figure 6: Histograms showing the distributions of a) early GM group video resolution, b) early GM group video FPS, c) late GM group video resolution, and d) late GM group video FPS

## B FURTHER RESULTS

Table 4 and Table 5 show the results of the presented classification models, for each labeller individually as well as averaged, grouped by age and feature extraction method used, measured in AUPRC and accuracy, respectively. The best performing method per task is marked in bold and overall both metrics resemble the behaviour of the AUROCs reported in the main text in Table 2.

Table 4: Results. **AUPRC** over 30 seeds is reported. The best result for each model and labeller is **bolded**.

Labeller	Features	Early GM Group			Late GM Group		
		RF	AUPRC LSTM	CNN	RF	AUPRC LSTM	CNN
1	Coord.	0.7733 ± 0.14	<b>0.7503 ± 0.13</b>	0.8585 ± 0.11	0.2589 ± 0.14	0.3603 ± 0.22	<b>0.4627 ± 0.23</b>
	Angles	<b>0.8856 ± 0.09</b>	0.7346 ± 0.16	<b>0.8772 ± 0.1</b>	<b>0.389 ± 0.25</b>	<b>0.47 ± 0.24</b>	0.266 ± 0.17
	Both	0.8575 ± 0.09	0.7359 ± 0.15	0.8547 ± 0.13	0.2879 ± 0.19	0.2938 ± 0.15	0.3983 ± 0.22
2	Coord.	0.665 ± 0.14	<b>0.7798 ± 0.14</b>	<b>0.799 ± 0.12</b>	0.3142 ± 0.18	0.38 ± 0.27	0.4778 ± 0.24
	Angles	<b>0.7703 ± 0.13</b>	0.7097 ± 0.17	0.6867 ± 0.16	<b>0.4674 ± 0.25</b>	<b>0.3814 ± 0.22</b>	<b>0.4959 ± 0.27</b>
	Both	0.7088 ± 0.15	0.7105 ± 0.15	0.7955 ± 0.14	0.3523 ± 0.18	0.3804 ± 0.22	0.4638 ± 0.25
3	Coord.	0.7259 ± 0.15	0.6986 ± 0.17	0.8522 ± 0.13	0.3593 ± 0.19	0.3405 ± 0.23	<b>0.5538 ± 0.21</b>
	Angles	<b>0.8685 ± 0.09</b>	0.6655 ± 0.16	0.85 ± 0.14	<b>0.4929 ± 0.28</b>	<b>0.4194 ± 0.24</b>	0.4061 ± 0.25
	Both	0.8121 ± 0.13	<b>0.7461 ± 0.17</b>	<b>0.8579 ± 0.12</b>	0.3603 ± 0.18	0.3838 ± 0.22	0.4269 ± 0.27
Mean	Coord.	0.7214	<b>0.7429</b>	<b>0.8366</b>	0.3108	0.3603	<b>0.4981</b>
	Angles	<b>0.8415</b>	0.7033	0.8046	<b>0.4498</b>	<b>0.4236</b>	0.3893
	Both	0.7928	0.7308	0.8360	0.3335	0.3527	0.4297
Automatic	Coord.	0.6324 ± 0.16	0.6969 ± 0.15	0.65 ± 0.15	0.3560 ± 0.21	0.5015 ± 0.24	0.4973 ± 0.25
	Angles	<b>0.6792 ± 0.15</b>	<b>0.7323 ± 0.16</b>	0.6546 ± 0.13	<b>0.3620 ± 0.19</b>	0.5765 ± 0.27	<b>0.6523 ± 0.28</b>
	Both	0.6340 ± 0.16	0.6451 ± 0.16	<b>0.6769 ± 0.15</b>	0.3340 ± 0.18	<b>0.5923 ± 0.28</b>	0.4504 ± 0.28

Table 5: Results. **Accuracy** over 30 seeds is reported. The best result for each model and labeller is **bolded**.

Labeller	Features	Early GM Group			Late GM Group		
		RF	Accuracy LSTM	CNN	RF	Accuracy LSTM	CNN
1	Coord.	0.5962 ± 0.16	0.59 ± 0.15	0.6946 ± 0.15	0.5759 ± 0.14	0.5793 ± 0.11	0.6133 ± 0.16
	Angles	<b>0.7266 ± 0.13</b>	0.5978 ± 0.14	<b>0.7047 ± 0.16</b>	<b>0.6305 ± 0.17</b>	<b>0.6785 ± 0.13</b>	0.5701 ± 0.13
	Both	0.6596 ± 0.15	<b>0.6444 ± 0.16</b>	0.6849 ± 0.12	0.6073 ± 0.16	0.5809 ± 0.16	<b>0.6168 ± 0.15</b>
2	Coord.	0.4542 ± 0.17	<b>0.5973 ± 0.15</b>	0.6219 ± 0.13	0.6385 ± 0.13	0.5856 ± 0.15	0.5603 ± 0.21
	Angles	<b>0.6518 ± 0.14</b>	0.5594 ± 0.14	0.5568 ± 0.17	<b>0.6765 ± 0.08</b>	0.6297 ± 0.14	<b>0.6432 ± 0.13</b>
	Both	0.5268 ± 0.18	0.5871 ± 0.16	<b>0.6275 ± 0.15</b>	0.6444 ± 0.13	<b>0.6418 ± 0.14</b>	0.6113 ± 0.16
3	Coord.	0.5548 ± 0.18	0.6125 ± 0.14	0.6764 ± 0.14	0.6652 ± 0.14	0.5955 ± 0.15	0.614 ± 0.19
	Angles	<b>0.6995 ± 0.11</b>	0.5443 ± 0.15	<b>0.7508 ± 0.12</b>	<b>0.6995 ± 0.08</b>	0.6233 ± 0.16	0.638 ± 0.12
	Both	0.6186 ± 0.17	<b>0.6502 ± 0.17</b>	0.7101 ± 0.14	0.6605 ± 0.09	<b>0.6505 ± 0.17</b>	<b>0.6393 ± 0.13</b>
Mean	Coord.	0.5351	0.5999	0.6643	0.6265	0.5868	0.5959
	Angles	<b>0.6926</b>	0.5672	0.6708	<b>0.6688</b>	<b>0.6438</b>	0.6171
	Both	0.6017	<b>0.6272</b>	<b>0.6742</b>	0.6374	0.6244	<b>0.6225</b>
Automatic	Coord.	0.4679 ± 0.13	0.5382 ± 0.16	0.4663 ± 0.15	0.5393 ± 0.17	0.599 ± 0.17	0.6236 ± 0.18
	Angles	<b>0.5015 ± 0.17</b>	<b>0.5907 ± 0.14</b>	0.4707 ± 0.11	<b>0.6185 ± 0.11</b>	<b>0.7131 ± 0.15</b>	<b>0.7048 ± 0.18</b>
	Both	0.4745 ± 0.15	0.5285 ± 0.20	<b>0.4879 ± 0.14</b>	0.5948 ± 0.14	0.6101 ± 0.18	0.6127 ± 0.19